Journal of Alloys and Compounds 645 (2015) S136–S139

Contents lists available at ScienceDirect

Journal of Alloys and Compounds

journal homepage: www.elsevier.com/locate/jalcom

High capacity hydrogen storage alloy negative electrodes for use in nickel–metal hydride batteries

Hiroshi Inoue *, Norihiro Kotani, Masanobu Chiku, Eiji Higuchi

Department of Applied Chemistry, Graduate School of Engineering, Osaka Prefecture University, Sakai, Osaka 599-8531, Japan

ARTICLE INFO

Article history:
Available online 28 January 2015

Keywords:
Electrode materials
Hydrogen-absorbing materials
Transition metal alloys and compounds
Crystal structure
Electrochemical reactions
Electrochemical impedance spectroscopy

ABSTRACT

Rare earth-free V-based $TiV_{2.1-x}Cr_xNi_{0.3}$ (x = 0.4–1.0) alloys were prepared by arc-melting. All alloys were composed of two phases, the primary phase in which the V and Cr constituents were mainly distributed and the secondary phase in which the Ti and Ni constituents were mainly distributed. When the Cr content was increased, the maximum discharge capacity was decreased, but charge–discharge cycle durability was improved. The lower the charge-transfer resistance and the higher the specific discharge current at which the positive shift of potential at degree of discharge of 50% stagnates, the higher the HRD. In the present study, the $TiV_{1.6}Cr_{0.5}Ni_{0.3}$ alloy electrode had the highest HRD.

1. Introduction

Rare earth-based AB_5-type hydrogen storage alloys and Mg-contained $AB_{3.3}$-type superlattice alloys are used as negative electrode active material for commercial nickel–metalhydride (Ni–MH) batteries. The low specific energy of the commercial Ni–MH batteries is a serious defect for current applications like mobile phone, vehicle, etc. For improving the specific energy, appearance of new hydrogen storage alloys with higher hydrogen storage capacity is particularly desirable. Meanwhile, the hydrogen storage alloys for commercial Ni–MH batteries include high contents of rare earth elements. The rare earth elements are available for not only hydrogen storage alloys but also magnetic and luminescent materials. However, they are produced in limited countries and not easily isolated. So the rare earth elements are often subject to speculation. Therefore, we have developed rare earth-free hydrogen storage alloys with high hydrogen capacity.

V-based hydrogen storage alloys with a body-centered cubic (bcc) structure as the primary phase have high gravimetric and volumetric hydrogen storage capacities, and therefore are potential candidates as negative electrode active material for Ni–MH batteries [1–8]. We found that the $TiV_{0.9}Ni_{0.5}$ electrode showed the highest discharge capacity (390 mA h g^{-1}) among the $TiV_{1.4-x}Ni_x$ ($0 \leqslant x \leqslant 1$) electrodes [9] and the $TiV_{2.1}Ni_{0.3}$ alloy, which was the primary phase of $TiV_{0.9}Ni_{0.5}$, had a much higher discharge capacity (540 mA h g^{-1}) than the original $TiV_{0.9}Ni_{0.5}$ alloy [10]. However, the $TiV_{2.1}Ni_{0.3}$ alloy exhibited poor charge–discharge cycle durability because of the dissolution of the V constituent in the 6 M KOH electrolyte solution. In order to suppress the deterioration of the $TiV_{2.1}Ni_{0.3}$ alloy, we tried various surface modification techniques, and elucidate their usefulness in terms of increasing maximum discharge capacity [11–15]. However, cycle performance was a little improved. The Cr-substitution of some hydrogen storage alloys was effective in improving cycle durability although their discharge capacity decreased [2,16,17]. We also prepared $TiV_{2.1-x}Cr_xNi_{0.3}$ (x = 0.1–0.4) alloys whose V constituent was partially substituted with Cr, and found they were effective for improving cycle stability [18]. In particular, the $TiV_{1.7}Cr_{0.4}Ni_{0.3}$ alloy was the best in terms of cycle stability and high-rate dischargeability. In this study we prepared $TiV_{2.1-x}Cr_xNi_{0.3}$ (x = 0.4, 0.5, 0.6 and 1.0) alloys and evaluated their electrochemical properties.

2. Experimental

$TiV_{2.1-x}Cr_xNi_{0.3}$ (x = 0.4, 0.5, 0.6 and 1.0) alloy ingots were prepared by arc-melting a mixture of Ti, V, Cr and Ni powders under an argon atmosphere [11]. Each alloy ingot was then put in a stainless steel reactor tube and broken with high pressure hydrogen. The coarsely broken alloys were further pulverized with a stainless steel mortar and pestle, and sieved to particle sizes of 25–106 μm.

The negative electrodes used in this work were prepared according to our previous procedure [11]. The electrolyte solution was 6 M KOH, and the positive and reference electrodes were NiOOH/$Ni(OH)_2$ and Hg/HgO electrodes, respectively. In charge–discharge cycle tests, each negative electrode was charged at 100 mA g^{-1} for 8 h and discharged at 50 mA g^{-1} to the cut-off potential of −0.75 V versus

* Corresponding author. Tel.: +81 722549283.
E-mail address: inoue-h@chem.osakafu-u.ac.jp (H. Inoue).

http://dx.doi.org/10.1016/j.jallcom.2015.01.132
0925-8388/

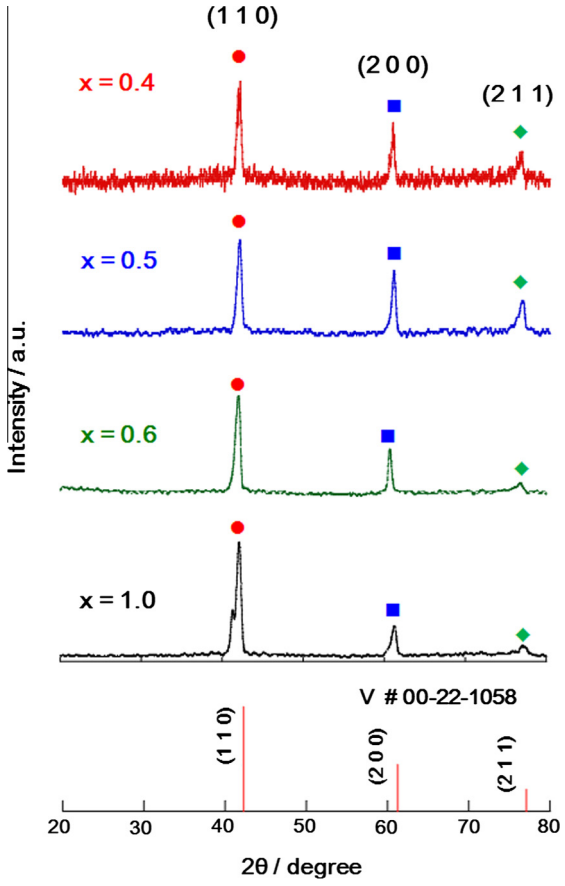

Fig. 1. XRD patterns for $TiV_{2.1-x}Cr_xNi_{0.3}$ (x = 0.4, 0.5, 0.6 and 1.0) alloy ingots.

Hg/HgO. After each charging, the circuit was kept open for 10 min. High-rate dischargeability (HRD) was measured at various specific current after charge–discharge cycles to the maximum discharge capacity. HRD (%) is evaluated from the following equation:

$$HRD = 100 \times (C_i/C_{25}) \quad (1)$$

where C_i and C_{25} are discharge capacity at i and 25 mA g^{-1}, respectively. AC impedance measurements were carried out at the degree of discharge (DOD) of 50% in the frequency range of 20 kHz to 0.01 Hz with the perturbation of 5 mV.

All electrochemical measurements were carried out at 303 K.

3. Results and discussion

X-ray diffraction spectra of $TiV_{2.1-x}Cr_xNi_{0.3}$ (x = 0.4, 0.5, 0.6 and 1.0) alloys are shown in Fig. 1. In this figure, all diffraction peaks for each alloy were assigned to the bcc structure. Each diffraction peak was shifted to the higher angles with increasing the Cr content. The lattice volume evaluated from each XRD pattern was 28.84 Å^3 for x = 0.4, 28.42 Å^3 for x = 0.5, 28.00 Å^3 for x = 0.6 and 27.85 Å^3 for x = 1.0. Thus the lattice volume of the primary phase was smaller for higher Cr content because the atomic radius of Cr was shorter than that of V.

Fig. 2 shows pictures taken by scanning electron microscopy (SEM) and maps of each constituent by electron dispersive X-ray (EDX) analysis for $TiV_{2.1-x}Cr_xNi_{0.3}$ (x = 0.4, 0.5, 0.6 and 1.0) alloys. The SEM images exhibited all alloys were composed of two phases, the primary and secondary phases, similar to the previously reported $TiV_{2.1}Ni_{0.3}$ alloy [2]. The EDX maps exhibited the V and Cr constituents were mainly distributed in the primary phase, while the Ti and Ni constituents were mainly distributed in the secondary phase. The compositions of the primary and secondary phases were evaluated from their EDX analysis [2,11], and summarized in Fig. 3. From this figure, the Cr constituent was mainly distributed in the primary phase, supporting the EDX mapping data in Fig. 2. The Cr content in both phases was increased with the x value. The V content in the primary phase was decreased with increasing the Cr content whose radius was shorter than that of V, supporting the higher angle shift of the X-ray diffraction peaks or the decrease in lattice volume. On the other hand, the Ti and Ni contents were high in the secondary phase, which supported the EDX mapping data in Fig. 2. In particular, the Ni content in the secondary phase was the highest for x = 0.5. The mole fraction of the primary phase for each alloy was evaluated according to Ref. [18], and it was 84.8%, 83.3%, 84.9% and 82.1% for x = 0.4, 0.5, 0.6 and 1.0, respectively. The mole fractions of the primary phases were similar irrespective of the Cr content, and much higher than those of the secondary phases.

Fig. 4(a) shows charge–discharge cycle performance of the $TiV_{2.1-x}Cr_xNi_{0.3}$ (x = 0.4, 0.5, 0.6 and 1.0) alloy electrodes. For the alloy electrodes with x = 0.4 and 0.5, the maximum discharge capacity was obtained at 2nd cycle, indicating that these electrodes had higher in initial activation than the alloy electrodes with x = 0.6 and 1.0. The maximum discharge capacity was decreased with increasing Cr content because the decrease in the V content in the primary phase due to the replacement with Cr leads to the decrease in lattice volume or hydrogen storage space. Average decrement in discharge capacity (ΔC_{dis}) from the maximum discharge capacity to discharge capacity at 30th cycle was 0.35% cycle^{-1} for x = 0.4 and 0.42% cycle^{-1} for x = 0.5, indicating that the former was superior in cycle stability to the latter. However, ΔC_{dis} value between 20th and 30th cycles was 0.36% cycle^{-1} for x = 0.4 and 0.09% cycle^{-1} for x = 0.5, indicating that cycle stability was inverse. In the latter, cycle life, cycle number required for the decrease in discharge capacity to a half of the maximum was more than 500 cycles, which was much longer than alloy electrodes with x = 0–0.3 [18]. For the alloy electrode with x = 1.0, discharge capacity was steadily increased for initial 20 cycles. However, the maximum discharge capacity was less than a half of that of the alloy electrodes with x = 0.4 and x = 0.5. In this way, the replacement of V with Cr leads to the decrease in the V content and the increase in the Cr content in the primary phase, causing the decrease in the improvement of cycle performance.

Fig. 4(b) shows HRDs of the $TiV_{2.1-x}Cr_xNi_{0.3}$ (x = 0.4, 0.5, 0.6 and 1.0) alloy electrodes. The alloy electrode with x = 1.0 was inferior in HRD to the other three electrodes. The HRDs of the alloy electrodes with x = 0.4, 0.5 and 0.6 were close to each other until specific discharge current of about 400 mA g^{-1}, which was better than the alloy electrodes with x = 0–0.3 [18]. But, over 400 mA g^{-1} the alloy electrode with x = 0.5 was a little superior to the other two electrodes.

Fig. 5(a) shows Nyquist plots at DOD = 50% for the $TiV_{2.1-x}Cr_xNi_{0.3}$ (x = 0.4, 0.5, 0.6 and 1.0) alloy electrodes. A charge-transfer resistance (R_{ct}) was evaluated from the semicircle in the low frequency range. This is assigned to charge transfer on the negative electrode active material, mainly the secondary phase of the alloy [1,18]. Consequently, R_{ct} was 1.46, 1.45, 1.49 and 1.60 Ω for x = 0.4, 0.5, 0.6 and 1.0, respectively. R_{ct} at x = 0.4, 0.5 and 0.6 was similar to each other. This seems to be related to the Ni content in the secondary phase as an electrocatalyst [1,18].

Fig. 5(b) shows potentials at DOD = 50% (E_{50}) measured from discharge curves with various specific discharge currents. For each alloy negative electrode, E_{50} was shifted in the positive direction as